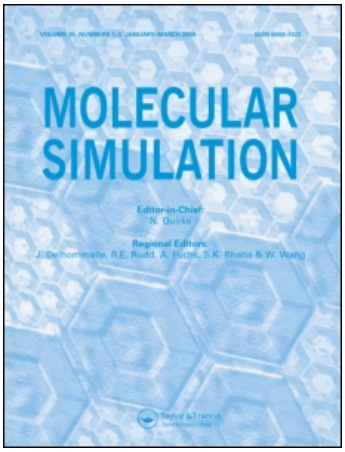


**Molecular Simulation**
Publication details, including instructions for authors and subscription information:
http://www.informaworld.com/smpp/title~content=t713644482

# Oligomers of Poly(Ethylene Oxide): Molecular Dynamics with a Polarizable Force Field

Jiř Kolafa[abc]; Mark Ratner[a]
[a] Department of Chemistry, Northwestern University, Illinois, U.S.A. [b] Lindø Center for Applied Mathematics, Odense M, Denmark [c] E. Hála Laboratory of Thermodynamics, Institute of Chemical Process Fundamental Acad. Sci., Prague 6-Suchdol, Czech Republic

**To cite this Article** Kolafa, Jiř and Ratner, Mark(1998) 'Oligomers of Poly(Ethylene Oxide): Molecular Dynamics with a Polarizable Force Field', Molecular Simulation, 21: 1, 1 — 26
**To link to this Article: DOI:** 10.1080/08927029808022047
**URL:** http://dx.doi.org/10.1080/08927029808022047

*Molecular Simulation*, 1998, Vol. 21, pp. 1–26
Reprints available directly from the publisher
Photocopying permitted by license only



# OLIGOMERS OF POLY(ETHYLENE OXIDE): MOLECULAR DYNAMICS WITH A POLARIZABLE FORCE FIELD

JIŘÍ KOLAFA [a,b,c,*] and MARK RATNER [a]

[a] *Northwestern University, Department of Chemistry, 2145 Sheridan Road, Illinois 60208-3113, U. S. A.;*
[b] *Lindø Center for Applied Mathematics, Forskerparken 10, DK-5230 Odense M, Denmark;*
[c] *E. Hála Laboratory of Thermodynamics, Institute of Chemical Process Fundamental Acad. Sci., 165 02 Prague 6-Suchdol, Czech Republic*

*(Received November 1997; accepted November 1997)*

A semi-empirical force-field for simulating oligomers of poly(ethylene oxide) is developed with the united atom representation for methyl and methylene groups. Polarizability of groups is mimicked by polarizable finite dipoles. The force field parameters are adjusted using both empirical data (density, dipole moments, dielectric constant) and *ab initio* calculations (dihedral torsion potentials, conformation energies). The molecular dynamics simulations make use of a novel predictor-corrector scheme for the self-consistent field, allowing only one evaluation of forces per integration step. Focus is on quantities related to ionic motion (dielectric constant and viscosity), the *gauche* effect, and methodology of simulations of complex polarizable molecules.

*Keywords:* Poly(ethylene oxide); force field; polarizability; molecular dynamics



## 1. INTRODUCTION

Poly(ethylene oxide), $CH_3—[CH_2—O—CH_2]_n—CH_3$ (also denoted as PEO or PEO*n*), has attracted considerable recent attention because of its ability to solvate ions and thus provide solid polymer electrolytes with many promising electrochemical applications, including high energy-density batteries [1–10]. The experimental findings have been followed by attempts

*Corresponding author.

to understand better the microscopic mechanisms using methods of computational statistical mechanics [11–18].

The molecular structure of PEO contains several peculiarities that must be considered in an accurate simulation force field. One of the most important is the low energy of *gauche* conformers of the internal rotation around $CH_2—CH_2$ bonds; the *gauche* minus *trans* difference in condensed phase has been estimated [19] as $-0.4$ kcal/mol. This so called *gauche* effect is present also for oligomers [20, 21] and has been, at least partly, reproduced by *ab initio* studies on molecules in vacuum [22, 25]. *Ab initio* calculations of the simplest nontrivial PEO homologue, dimethoxyethane $H—[CH_2—O—CH_2]_2—H$ or DME, immersed in a dielectric continuum [26, 27] followed by a molecular dynamics study [28] reveals further stabilization of the *gauche* conformer in a polarizable environment. The high stability of the $tg^+g^-$ conformer of DME [22, 23] caused by close contact of negative oxygen and positive $CH_3$ group (with a possible weak hydrogen bond [24]) is probably of lower importance in bulk PEO since intermolecular $CH_3\cdots O$ interactions may take place instead.

The anisotropic electronic distribution about oxygen in these ethers, plus their remarkable solvating ability, suggest that polarization of the ether by the cation might be an important component of solvation and complex formation. This in turn suggests that accurate simulations will require such polarization effects. In this contribution, we develop and test just such a polarizable force field, and methods for its efficient utilization.

Several molecular simulation calculations on PEO and its oligomers have been reported. Some earlier works [18, 29] use general molecular dynamics/force field packages, which limits their capability to describe the phenomena mentioned above, the weakest point being the dihedral potentials.

The force field used by Müller-Plathe and coworkers [14, 30, 31] is tailored to PEO. It is based on the usual Lennard-Jones atom-atom terms (all atoms including hydrogens are present) and partial charges obtained from *ab initio* calculations on DME. The same system is used to develop the dihedral potentials.

The force field developed by Neyertz and co-workers [13] is based on crystalline PEO as the benchmark system, and was applied to a crystalline complex $PEO_3NaI$ [32]. The amorphous phase of both PEO [33] and $PEO_3NaI$ [34] was built by the pivot Monte Carlo method and studied further by molecular dynamics. In this force field the Lennard-Jones terms are replaced by a Buckingham (exp-6) site-site potential. The *ab initio* fits to dihedral energies [25] were used as dihedral potential terms without correcting for non-bonded intra-chain interactions (turned on at the 1–5

term, cf. Section 2.5); since these terms are attractive, the potential exaggerates the *gauche* effect.

The force field for DME used in Monte Carlo simulations [35] is a TIPS or OPLS type force field with united atom representation for methyl and methylene groups. The *gauche* effect in the liquid phase is correctly reproduced. Similar results are obtained by molecular dynamics calculations [36, 24] using an *ab initio* based interaction potential [37] with explicit hydrogens.

All these force fields are pairwise additive. The dielectric properties of the liquid phase are introduced only by rearranging molecular dipoles, and thus the partial charges are generally quite high to correct for missing polarizability at the atomic level [38–41]. Since it is believed that polarizability plays an important role in phenomena like solvation of ions and dielectric properties, we present and test what we believe to be a more accurate approximation of the electrostatic force field, specifically including dipolar polarizability of interactions sites in the potential model (Section 2). Works using polarizable force fields for molecules of similar complexity are still rare. To facilitate efficient use of such a force field, we present (Section 3 and Appendix A) a predictor-corrector integrator that minimizes the computational overhead. Results are given in Section 4.



## 2. THE POLARIZABLE UNITED-ATOM FORCE FIELD (PUFF)

The etheric oxygen in oligoethers and polyethers acts as a Lewis base. The electron cloud around the O center is polarizable, and this polarizability should be important in complexation of cations, as stressed recently [42] in a combined study of cation/ether complexes using mass spectroscopy and quantum chemistry. Therefore, a polarizable force field should be valuable in MD simulations of such species. This paper is devoted to development and testing of such a potential.

The choice of the force field is always a compromise between accuracy and simplicity. In order to keep the complexity of our first attempt at a complex polarizable force field minimal, we have chosen the united atom representation for groups $CH_3$ and $CH_2$. It can be estimated [43] that adding explicit (non-polarizable) hydrogens would increase the computational overhead (with Ewald summation) more than 2 times. We refer to the resulting force field as the PUFF force field.

### 2.1. Molecular Geometry and Bending Potentials

The bond lengths are 1.43 Å for C—O bonds, 1.54 Å $CH_2$—$CH_2$ bonds and 1.516 Å for $CH_3$—$CH_2$ bonds [19, 44]; for the sake of simplicity we do not adopt suggested slightly lower values 1.41 - 1.42 Å for C—O bonds in ethers [44]. The bond lengths are constrained. The equilibrium bond angels are $\theta_0 = 110°$ for C—C—O and 112° for C—O—C with the bending potential given by

$$U_{\text{bend}}(\theta) = K(\theta - \theta_0)^2 \tag{1}$$

For the force constants $K$ we adopt the values of CHARMM [45], $K_{C-C-O} = 80\,\text{kcal/mol/rad}^2$ and $K_{C-O-C} = 70$ kcal/mol/rad$^2$ which lie, approximately, between the values used by other force fields [13, 14, 46].

### 2.2. Lennard-Jones Parameters

The Lennard-Jones potential is defined by

$$u(r) = 4\varepsilon[(\sigma/r)^{12} - (\sigma/r)^6] \tag{2}$$

where $r$ is the distance between interacting sites.

Several parameterizations of LJ parameters for groups are available [44, 45, 47–50], see Table I. These are adjusted using different sets of substances as well as different combining rules for interactions of unlike sites. The majority of force fields use (rather counterintuitively) a smaller diameter for $CH_3$ than for $CH_2$, with the only exception being OPLS adjusted to

TABLE I LJ parameters for groups. The Lennard-Jones $\sigma$ is in Å (1 Å = 0.1 nm), the energy $\varepsilon$ in kcal/mol (1 kcal = 4184 J)

| *group* | *PUFF* | | *OPLS* [44] | | *CHARMM* [45] | | *TIPS* [49] | | *UNICEPP* [50] | |
|---|---|---|---|---|---|---|---|---|---|---|
| | $\sigma$ | $\varepsilon$ | $\sigma$ | $\varepsilon$ | $\sigma$ | $\varepsilon$ | $\sigma$ | $\varepsilon$ | $\sigma$ | $\varepsilon$ |
| $CH_3$[a] | 3.85 | 0.175 | 3.905 | 0.175 | 3.858 | 0.181 | 3.861 | 0.181 | 3.79 | 0.18 |
| $CH_3$[b] | 3.75 | 0.175 | 3.8 | 0.18 | | | | | | |
| $CH_2$ | 3.95 | 0.115 | 3.8 | 0.118 | 3.982 | 0.114 | 3.983 | 0.114 | 3.96 | 0.14 |
| O | 3 | 0.17 | 3 | 0.170 | 2.851 | 0.159 | 3.047 | 0.195 | 3.118 [51] | 0.06 [51] |
| intrachain: | | | | | | | | | | |
| 1-4 | no | | yes | | scaled | | yes | | yes | |
| 1-5 | scaled | | yes | | yes | | yes | | yes | |

[a] in ethyl.
[b] in methylether.

substances most similar to PEO, alkyl ethers. However, our simulations with this force field and higher PEO oligomers lead to densities overestimated by more than 10%. If we do not want to change the oxygen value, the diameter of intrachain $CH_2$ must be increased. To reproduce the experimental densities, consistent usage of this $CH_2$ also in the ethyl group then requires smaller diameters for both types of $CH_3$. We do not adjust the energy parameters.

For interactions of unlike sites the combining rule must be defined. For the LJ diameters we adopt the geometric mean,

$$\sigma_{ij} = \sqrt{\sigma_i \sigma_j} \tag{3}$$

as in TIPS and OPLS. Since we will use group polarizabilities anyway, the natural choice for the energetic combining rule is the Slater-Kirwood formula [48, 50]:

$$\varepsilon_{ij} = \alpha_i \alpha_j \sigma_{ij}^{-6} / (\gamma_i + \gamma_j) \tag{4}$$

where

$$\gamma_i = \alpha_i^2 / (2\varepsilon_i \sigma_i^6) \tag{5}$$

and $\alpha_i$ denotes the scalar polarizability. These values apply for sites on different molecules and 1–6 or more distant sites on one chain. See below for special 1–5 terms.



### 2.3. Polarizabilities

In this paper we approximate the polarizability effect on groups by dipolar isotropic polarizability only. The polarizability tensor is thus diagonal and may be replaced by scalar polarizability. Since the induced dipole is modeled by finite dipole, the response is not exactly linear, as discussed in Section 3.

Linear regression of data for alkanes (see Table II) gives the value of the polarizability of the methylene group as approximately 1.85 Å$^3$. Methyl (1/2 of ethane) has 2.225 Å$^3$. By subtracting two methyls from the polarizability of dimethylether we get the ether oxygen value as 0.775 Å$^3$. The final rounded values and predicted polarizabilities of different substances are collected in Table II. The estimated polarizability of our test substance, dimethoxyethane, lies between the *ab initio* values without and with the conformational part of polarizability (as it should, because some of the

TABLE II Polarizabilities (in Å$^3$) of simple molecules and groups

| | *exptl.* [66] | *PUFF* |
|---|---|---|
| $CH_3$ | | 2.2 |
| $CH_2$ | | 1.85 |
| O | | 0.8 |
| methane | 2.593 | 2.55 |
| ethane | 4.43; 4.47 | 4.4 |
| propane | 6.29; 6.37 | 6.25 |
| *n*-butane | 8.20 | 8.1 |
| *n*-pentane | 9.99 | 9.95 |
| *n*-dodecane | 22.8 | 22.9 |
| dimethylether | 5.16; 5.29; 5.84 | 5.2 |
| diethylether | 10.2; 8.73 | 8.9 |
| DME [a] | 7.53; 10.1 | 9.7 |

[a] *ab initio* values [26]. The first value is static electron polarizability, the second includes the conformational polarizability.

conformational degrees of freedom are taken into account by the model but some, such as rotations of the methyl groups, are not).



## 2.4. Partial Charges

The experimental dipole moment for diamethylether, 1.30 D, along with the molecule geometry, suggests that the partial charge of oxygen should be $-0.34e$ (and $+0.17e$ for each methyl group), while analysis of dipole moments of higher aliphatic ethers leads to a slightly lower value [19] of $-0.31e$. The OPLS model [44] uses $-0.5e$ for the diethylether oxygen, which gives too high a dielectric constant even if the polarizability is not included, and the more recent united atom MC model [35] uses $-0.44e$. Quantum mechanical calculations on DME lead to [14] $-0.348e$ for a full-atom model (charge of C $0.103e$, charge of H $0.0355e$), which would correspond to a slightly higher equivalent value for a united atom model to reproduce the dipole moments along the chain.

Neither of these values was derived with polarizability in mind. Pairwise-additive force fields usually increase the values of partial charges (and hence gas-phase molecular dipole moments) to account for induced dipoles, and thus charges have to be scaled down [38–41] in polarizable force fields.

Our value of the oxygen charge $-0.3e$ is lower than the above literature data. It was fitted chiefly to the dielectric constants of PEO oligomers. The charge of methylenes and methyls adjacent to oxygen are thus $0.15e$, while the charge of methyl in the ethylether group is zero. The experimental value of dipole moment of diethylether (1.15 D at 25° C) is well reproduced by our model (1.156 D).

### 2.5. Dihedral Potentials and Non-bonded Offset

The dihedral angle $\phi$ for four atoms A–B–C–D in chain, called also the (proper) torsion angle or internal rotation angle, is defined as the oriented angle between planes ABC and BCD so that $\phi = 0$ for the *cis* conformation. The dihedral potential up to the sixth Fourier coefficient, rewritten for computational convenience in powers of cos $\phi$, reads

$$U(\phi) = \sum_{n=0}^{6} a_n \cos^n \phi \tag{6}$$

There are two basic strategies to describe the torsional potentials in the molecule (cf. Table I). One approach [14, 48, 51] leaves (possibly modified) 1–4 non-bonded interactions (i.e., interactions of atoms separated by 3 bonds) which thus generate a part of the torsional barrier. The explicit dihedral potential may be thus simpler and may contain, if we take the $CH_2$-$CH_2$ bond as example, only $\cos(3\phi)$ terms. The other approach [35, 44] omits any 1–4 non-bonded interactions which are described indirectly by a more complicated dihedral potential. It should be stressed that both approaches are equivalent as regards the resulting effective rotational potential — provided that the force field is pairwise additive.

These two approaches are no longer equivalent if the force field is polarizable, because the 1–4 charge-charge terms cause internal polarization which is felt by other molecules (and distant atoms in the same molecule) and which is not constant because the 1–4 distances change by internal rotations. (On the other hand, the 1–2 and 1–3 distances vary only marginally and these terms could cause only almost constant charge redistribution; thus it does not make sense to consider them because the static charge distribution is by definition described by a static distribution of partial charges). Since the 1–4 sites are close together, the full Coulomb interaction could even cause the polarization catastrophe (divergence of the self-consistent field equations). Our choice to neglect the 1–4 terms is thus motivated more by simplicity than by physical intuition, which says that the intramolecular 1–4 polarization should not be totally neglected but included (perhaps multiplied by a certain factor).

While the 1–2, 1–3, and 1–4 non-bonded terms are neglected and 1–6 and more distant are included in their full form, we had to adjust the 1–5 LJ terms to achieve better agreement for the $tg^+g^-$conformer of DME. Without this correction, the C···O distance is too large and the $tg^+g^-$ conformer is not sufficiently stabilized by intramolecular Coulomb

interaction. This 'potential patch' may be considered as a drawback of the united atom approximation which cannot describe the close O···H intramolecular interaction. The best conformational energy has been obtained by scaling the combining rule diameter for $CH_2$—O non-bonded interaction by a factor $q = 0.86$ and then the energy term by $q^3$; for the sake of internal consistency of the PUFF force field, we rescale all 1–5 interactions by the same factors.

As the starting point for developing the dihedral potentials, we use the parameterized energies [25] of different conformers of diglyme H—$[CH_2—O—CH_2]_3$—H), see Table III. This energy is to be reproduced by a sum of dihedral potentials and 1–5, 1–6, etc., non-bounded terms. Since the non-bonded terms are known, the dihedral terms can be derived. In these calculations we approximated the optimized geometry (for all degrees of freedom except the investigated dihedral angle): The values of all *trans* dihedral angles are exactly 180° and all bond angles equal their equilibrium values; calculations with the resulting force field show that the maximum error of this approach is roughly 0.02 kcal/mol.



## 3. SIMULATION METHODOLOGY

For models with partial charges it appears to be computationally convenient to replace polarizable point dipoles by pairs of charges of opposite signs close togther. A charge $ne$, where $n$ is the number of outer shell electrons ($n = 7$ for $CH_3$, $n = 6$ for $CH_2$ and O), is added to the polarizable site (which already has some partial charge). The additional charge is compensated by negative charge $-ne$ whose position $\mathbf{r}_i$ relative to the site

TABLE III Dihedral potentials as polynomials in the cosine of the dihedral angle. $E$ in the first lines are fits to *ab initio* energies of DME conformers [25], the values in the second lines are the derived PUFF dihedral potentials normalized to zero at the *trans* conformation. All values are in kcal/mol

| | $a_0$ | $a_1$ | $a_2$ | $a_3$ | $a_4$ | $a_5$ | $a_6$ |
|---|---|---|---|---|---|---|---|
| $E_{\phi ttt}$ | 1.4589 | −1.2459 | 1.8629 | 3.9254 | −1.0633 | 0.9981 | 1.4150 |
| $CH_3—O—CH_2—CH_2$ | 1.6988 | −0.9625 | 1.9201 | 3.9368 | −1.0619 | 0.9968 | 1.4141 |
| $E_{t\phi tt}$ | 0.5280 | −3.6300 | 4.2634 | 7.7552 | −3.3156 | 0.2830 | 2.9446 |
| $O—CH_2—CH_2—O$ | 1.2295 | −2.7652 | 4.4493 | 7.7982 | −3.3055 | 0.2853 | 2.9450 |
| $E_{tt\phi t}$ | 1.2385 | −1.3403 | 1.4957 | 3.6854 | −0.1568 | 1.0899 | 0.8490 |
| $CH_x—CH_2—O—CH_2$ | 1.5556 | −0.9481 | 1.6017 | 3.7128 | −0.1514 | 1.0896 | 0.8483 |

is derived from the electrostatic force $\mathbf{F}_i$ acting on it in the same way as in the general Eq. (12) of Appendix A:

$$\mathbf{r}_i = \frac{\alpha_i}{n^2 e^2} \mathbf{F}_i \tag{7}$$

The bulk-fluid simulations were run in the usual cubic periodic boundary conditions. Electrostatic interactions were calculated by the Ewald summation [52, 53]. The Ewald parameters, $\alpha_{\text{Ewald}}$ and the reciprocal-space cutoff $K$, were determined from approximate error formulas [43] where only the partial charges and no auxiliary dipolar charges are taken into account. This is possible due to the fact that (1) induced dipoles are smaller than or at worst comparable to the permanent dipoles, and (2) the real-space energy terms are calculated whenever the separation of the atoms is less than the cutoff, irrespective of the distance of auxiliary charges, and thus no errors caused by subtracting two large numbers may appear. The estimated maximum real space cutoff error of forces acting on maximum charge was $10^{-4}$ kcal/mol/Å while for the reciprocal space errors we allow a value ten times higher (but the actual reciprocal space error for our system without free charges is expected to be several times lower [43]). The error conditions give two equations for three parameters of the Ewald summation (real and reciprocal space cutoffs, $r_c$ and $K$, and the separation parameter $\alpha$). The third condition is equality of CPU times for both real (including other pair interactions) and reciprocal parts of the Ewald sum; this ensures the best load-balance on a mulitprocessor computer using two parallel threads. For instance, the simulation of 75 molecules of PEO3 uses $r_c = 13.3$ Å, $K = 5.79$, $\alpha = 0.237$/Å.

The equations of motions for bulk-fluid molecular dynamics are integrated by the Verlet method with the bond lengths constrained by SHAKE [52]. For the self-consistent field the novel predictor-corrector method described briefly in Appendix A is applied. Using the convergence properties of the self-consistent field equation and the theory described in detail in [54] we have estimated that the value $\omega = 0.72$ of the mixing iteration parameter of Eq. (15) can be safely used for PEO in normal conditions.

The temperature was kept constant by the friction thermostat [52] with the effective relaxation time of 1ps (more precisely, the correlation time would be 1 ps if the heat capacity were $k_B$ per degree of freedom) and similarly the pressure was kept at 1 bar by a friction-like rescaling of the simulation box with a time constant which would be 100 ps for an ideal gas but will be shorter (proportional to the compressibility) for bulk fluid. It is still long enough not to affect significantly the system; this can be verified

using the difference between the intermolecular and intramolecular kinetic temperatures (defined by kinetic energies of the centers of mass and center-of-mass reduced parts, respectively, reduced by the respective numbers of degrees of freedom) which did not exceed $1.5 \pm 0.5$ K. The productive runs lasted at least 1 ns (500,000 steps of 2 fs).

To calculate shear viscosities, both equilibrium (based on Green-Kubo theory) and non-equilibrium molecular dynamics (NEMD) methods are available and widely used [52, 55]. The NEMD method comes in two flavors: one is based on introducing a shear velocity profile (e.g., SLLOD [55, 56]) and measuring the off-diagonal elements of the pressure tensor, and the other applies a shear force instead and the velocity profile is measured. Becuase of methodological problems with determining the pressure tensor for a non-additive force field, we have chosen the latter method.

In our work a $z$-periodic shear stress was applied in the direction of $(x, y, z) = (2^{-1/2}, 2^{-1/2}, 0)$ according to the formula [52] for the force on atom $i$ having mass $m_i$

$$f_i = m_i C_a \cos(2\pi z/L) \tag{8}$$

where $L$ is the box size. To facilitate comparison of systems with different sizes, we write the acceleration constant $C_a$ in the form

$$C_a = \sqrt{\frac{8\pi^2 Q N_f k_B}{\rho^2 L^5}} \tag{9}$$

where $N_f$ is the total number of degrees of freedom in the system and $\rho$ the mass density. Parameter $Q$ has a physical meaning of $Q = \eta \dot{T}$ where $\eta$ is the (estimate of) viscosity and $\dot{T} = dT/dt$ the expected heating rate (assuming, as above, the heat capacity of $k_B$ per degree of freedom). The heat generated by friction was absorbed by the friction thermostat with time constant 0.6 ps.

Two auxiliary quantities were monitored to control proper pseudoexperimental conditions: the difference $\Delta T$ between inter- and intramolecular temperatures and cross sections $S$ measured in three directions, $x+y$, $x-y$, and $z$. The cross section is defined as the area of projection of the molecule, all atoms in a molecule being replaced by spheres with diameters given by Lennard-Jones $\sigma$. This area was calculated on a rectangular grid with resolution 0.1 Å.

The relative dielectric constants were obtained from fluctuations of the total dipole moment $\mathbf{M}$ by the generalized fluctuation formula (27) derived

in Appendix C. The value of the relative dielectric constant of the continuum surrounding the simulation box at infinity [53] was set to $\varepsilon' = 4$. Test calculations of liquid DME and $\varepsilon' = 1, 4, 10$ showed that the calculated dielectric constants do not depend (within statistical inaccuracy of about $\pm 1$) on the value of $\varepsilon'$.

Results for the dilute gas were obtained by the Nosé canonical thermostat [57] applied to one molecule in free boundary conditions (vacuum). Note that the friction thermostat cannot be used because it does not give a sufficiently accurate approximation of the canonical distribution for systems with a small number of degrees of freedom. Experience shows that our five and six atom systems with Nosé are complex enough to be ergodic (the only problems have been experience for diethylether with constrained bond angles).

Since MD simulation on a single molecule conserves the angular momentum, the method described above does not sample the whole phase space but only the subspace of constant angular momentum. We set this angular momentum to zero and corrected it during the MD run for numerical errors. The expected systematic difference between the true canonical ensemble and the restricted zero-angular-momentum canonical ensemble was estimated by calculations using a simplified force field (bond angles constrained and no polarizability), see Table V. The details of the method are given in Appendix B. Constraining the bond angles is a more serious approximation than constraining bond lengths, and significant differences in e.g., the dihedral angle distribution may be observed [58]. Due to fortuitous cancellations (flexible bond angles allow for lower energy of especially *gauche* conformers, which is not possible for rigid angles; dynamic effects also prefer *gauche* conformers) this difference is a few percent for DME and since we use the simplified force field only to estimate a small correction, we consider this approach as acceptable.

Because of technical problems in involving simultaneous use of the Nosé method and Verlet integrator (the right-hand side of the equations of motion depends on velocities), for single molecule calculations we used the fourth-value Gear predictor-corrector integrator [52] with constraint forces calculated by Lagrange multipliers [59]. The same predictor as in the Gear method was used also for the self-consistent field. Such a predictor is generally unstable [54] and thus the self-consistent solution was obtained by iterating [60] until a sufficient precision was reached; for these one-molecule systems this rarely required more than one iteration.

The local energetic minima of conformers were obtained by simulated annealing. A free molecule in vacuum was simulated with friction thermostat, cooling slowly to $T = 0.01$ K.

## 4. RESULTS AND DISCUSSION

### 4.1. Conformational Analysis of Dimethoxyethane

As mentioned above, the intramolecular 1–5 terms have been adjusted to the energy of the $tg^+g^-$ conformer of DME. Data have been taken from an accurate *ab initio* study [22] on the MP2/D95+(2df, p) level for which the authors claim a maximum energy error of 0.2–0.3 kcal/mol. Energies and dipole moments of all conformers of DME calculated with our force field are compared in Table IV with the *ab initio* values. The *ttt* conformer is taken as the reference and has zero energy by definition.

It is seen that the energies of both the *tgt* and *ttg* conformers are in a good agreement with the *ab initio* values. This means that our strategy for developing the dihedral potentials is sensible and independent of chain length.

The agreement is worse for multiple-*gauche* conformers, especially for the $g^+g^+g^+$ one. For this conformer this sample HF calculation also gives a worse result. The $CH_3$ groups are so bulky so that they destabilize the $g^+g^-g^+$ conformer; this conformer can be artificially stabilized by rescaling the $CH_3$ diameter by about 0.9.

The gas-phase value of dipole moment serves as a demanding test of both partial charges and dihedral potentials. We have calculated it from the formula

$$\bar{\mu} = \langle \mu(t)^2 \rangle^{1/2} \tag{10}$$

where the angle brackets denote the canonical expection value. A 0.1 μs run for a single molecule, corrected for the systematic error caused by

TABLE IV Energies and dipole moments of dimethoxyethane conformers. Note that the $tg^+g^-$ energy was used to adjust the 1–5 interactions (1 Debye = $3.33564\times10^{-30}$ C m.)

| *conformer* | $E-E_{ttt}$[*kcal/mol*] | | μ [*Debye*] | |
|---|---|---|---|---|
| | *PUFF* | *Ref.* [22] | *PUFF* | *Ref.* [22] |
| *ttt* | 0 | 0 | 0 | 0 |
| *tgt* | 0.15 | 0.10–0.4 | 1.42 | 1.52 |
| $tg^+g^+$ | 1.51 | 1.51 | 2.20 | 2.67 |
| $tg^+g^-$ | 0.23 | 0.23 | 1.69 | 1.65 |
| *ttg* | 1.35 | 1.43 | 1.39 | 1.93 |
| $g^+tg^+$ | 2.73 | 3.13 | 1.72 | 2.44 |
| $g^+tg^-$ | 2.57 | 3.08 | 0 | 0 |
| $g^+g^+g^+$ | 2.68 | 1.64 | 1.90 | 1.49 |
| $g^+g^+g^-$ | 1.89 | 1.86 | 1.83 | 2.10 |
| $g^+g^-g^+$ | unstable | 2.41 | unstable | 0.09 |

conserving angular momentum in MD (see Appendix B and Table V) gives $\bar{\mu} = 1.386 \pm 0.007$D at 25°C, which is lower than both the experimental values 1.59 – 1.75 D in various nonpolar solvants and an *ab initio* result [22] 1.58 D. This supports the observation [38–41] that dipolar polarizable models exaggerate the role of polarizability and thus partial charges must be lower to reproduce dielectric properties (though this rescaling is not so large as that occuring in pairwise additive models).

### 4.2. Thermodynamic Results

The experimental values for densities and dielectric constants of Table VI can be compared in Table VII with the molecular dynamics results.

The densities were used to adjust the Lennard-Jones diameters for groups and are thus reproduced with high precision, comparable to inaccuracies achieved by other force fields built up on similar principles [44, 49].

The dielectric constant is difficult to measure in molecular simulation calculations because it is derived from fluctuations of one global quantity. In addition, its value depends strongly on partial charges, details of charge distribution in the molecule, and certainly also on conformational energies. It is thus seen from Table VII that the model is not able to reproduce such details as lower dielectric constant of PEO2 compared to both PEO1 and PEO3, though the trend of increasing the dielectric constant with chain length is discernible.



TABLE V Calculated gas phase dipole moments of dimethoxyethane by different methods

| *bond angles* | *polarizability* | *angular momentum* | *calc. method* | $\bar{\mu}$ [*Debye*] |
|---|---|---|---|---|
| bending | yes | zero | MD | 1.367(7) |
| fixed | no | zero | MD | 1.326(5) |
| fixed | no | zero | integration | 1.322 |
| fixed | no | canonical | integration | 1.341 |

TABLE VI Experimental properties of PEO oligomers at 20°C. $\rho$ denotes the density, $\eta$ shear viscosity (Pa s = 10 Poise) and $\varepsilon_r$ is the dielectric constant (relative to vacuum) [67]

| *formula* | *name* | $\rho$ *kg* $m^{-3}$ | $\eta$ *mPa s* | $\varepsilon_r$ |
|---|---|---|---|---|
| $C_4H_{10}O$ | diethyl ether (PEO1) | 713.8 | 0.234[a] | 4.27 |
| $C_6H_{14}O_2$ | ethylene glycol diethyl ether (PEO2) | 848.4 | 0.70 | 3.90 |
| $C_8H_{18}O_3$ | diethylene glycol diethyl ether (PEO3) | 906.3 | 1.40 | 5.70 |
| $C_4H_{10}O_2$ | dimethoxyethane (DME) | 869.1 | 0.455[b] | 7.30[c] |
| $C_6H_{14}O_3$ | diglyme | 943.4 | 0.989[b] | |

[a] interpolated (log $\eta$ vs. $1/T$).
[b] 25° C.
[c] 24° C.

TABLE VII Molecular dynamics results on various PEO oligomers in liquid phase at 0.1 MPa and 20°C. $N$ denotes the number of molecules in the sample, $R^g$ is the radius of gyration, $R_{CH_3-CH_3}$ the mean quadratic end-to-end distance. For the explanation of the remaining symbols see Table VI. The values in parentheses are the estimated errors (standard deviations of the average) in units of the last significant digit

| *name* | $N$ | $\rho$ kg m$^{-3}$ | $\varepsilon_r$ | $R^g$ Å | $R_{CH_3-CH_3}$ Å |
|---|---|---|---|---|---|
| PEO1 | 128 | 712.7(6) | 4.27(10) | 1.7125(2) | 4.652(1) |
| PEO2 | 90 | 844.2(4) | 4.9(3) | 2.476(2) | 6.951(9) |
| PEO3 | 75 | 913.0(4) | 5.8(3) | 3.157(5) | 8.88(1) |
| PEO6 | 50 | 1006.1(6) | 6.4(7) | 4.82(2) | 13.2(1) |
| DME | 100 | 854.8(6) | 6.2(3) | 1.916(2) | 5.188(9) |
| diglyme | 92 | 942.4(4) | 6.6(4) | 2.678(5) | 7.41(2) |

On the other hand, a similar but non-polarizable united-atom model of DME [35] gives (according to our calculations) too high a dielectric constant $\varepsilon_r = 10.0 \pm 0.4$, a consequence of high partial charges which have to take into account the missing polarizability.

Unlike the above quantities, which can be reliably measured in single runs and moderately large system, the NEMD shear viscosities generally require extrapolation to zero value of the stress force and, in the method using periodic stress force, its gradient ($k$-vector or system size). This would require an unfeasible number of simulation runs, so that we choose a cheaper strategy. First, preliminary runs showed that the use of small systems of Table VII (in addition to possible errors caused by too high $z$-direction wave vector) does not allow a good choice of the shear stress amplitude: High values of the stress orient the molecules in the direction of the stress, but with low values the velocity profile is not discernible in thermal motion. This is in accordance with observations on liquid butane [61, 62].

Runs on moderately large system of DME, see Table VIII, show systematic increase of the estimated viscosities with decreasing value of the stress in accordance with simulations and theory [55] predicting linear dependence of viscosity on the square root of the stress (fourth root of $Q$). This is confirmed for PEO3, but not for the least accurate results of PEO1. Nevertheless, the results allow us to estimate the systematic underestimation of viscosity of our data obtained with lowest $Q$ to be about 10%. In addition, no system-size dependence is found. Further evidence about the viscosity-stress dependence comes from comparison with recent accurate MD data for a united-atom model of decane [56]. The strain rate (gradient of velocity) is expressed in this paper by a dimensionless quantity

$$\gamma = (m\sigma^2\varepsilon)^{1/2} \mathrm{d}v_{x+y}/\mathrm{d}z \tag{11}$$

TABLE VIII Molecular dynamics results for shear viscosity $\eta$. $Q$ denotes the shear stress parameter (see Eq. (9)), $S_{x+y}$ is the molecular corss section in the direction of stress force $S_z$ in the direction of its gradient, and $S_{x-y}$ in the perpendicular direction and $\Delta T$ is the difference inter- and intramolecular kinetic temperatures

| *name* | $N$ | $Q$ $10^{-6}$ *kg K* $m^{-1}s^{-2}$ | $\eta$ *mPa s* | $S_{x+y}$ $\AA^2$ | $S_{x-y}$ $\AA^2$ | $S_z$ $\AA^2$ | $\Delta T$ *K* |
|---|---|---|---|---|---|---|---|
| PEO1 | 256 | 375 | 0.190(6) | 27.35(6) | 27.59(4) | 27.58(8) | 4.0(9) |
| PEO1 | 256 | 94 | 0.172(9) | 27.42(2) | 27.53(4) | 27.55(4) | 2.5(6) |
| PEO1 | 512 | 94 | 0.199(9) | 27.42(3) | 27.52(2) | 27.56(3) | 1.0(5) |
| PEO2 | 720 | 47 | 0.44(3) | 38.00(4) | 38.33(6) | 38.43(7) | 0.5(7) |
| PEO3 | 600 | 625 | 0.69(2) | 47.11(11)[a] | 48.94(10)[a] | 50.11(8) | 3.9(7) |
| PEO3 | 600 | 156 | 0.77(5) | 47.83(11)[a] | 48.90(8)[a] | 49.29(6) | 0.3(7) |
| DME | 200 | 2000 | 0.227(6) | 28.37(7) | 29.49(6) | 29.73(7) | 20.2(14) |
| DME | 200 | 1000 | 0.249(7) | 28.63(8) | 29.34(9) | 29.70(7) | 11.9(13) |
| DME | 200 | 250 | 0.260(9) | 29.11(4) | 29.27(6) | 29.24(5) | 1.3(10) |
| DME | 400 | 62 | 0.268(11) | 29.26(4) | 29.18(3) | 29.17(5) | 1.1(5) |
| diglyme | 736 | 125 | 0.60(4) | 39.74(9) | 40.13(4) | 39.87(11) | −0.2(9) |

[a] The error is probably underestimated becuase of poor convergence (long correlation time).



where $m$ is the mass and $\sigma$ and $\varepsilon$ the Lennard-Jones parameters of the $CH_2$ group. Direct link to our work is impossible because of several types of atoms and additional electrostatic forces, but if we average the Lennard-Jones interactions of our model and take the maximum of the $z$-varying stress, we arrive at $\gamma^{1/2} \approx 0.2$ for the best (lowest shear rate) data. Comparison with decane results [56] suggest about 10% underestimation.

Additional information comes from the measured cross-sections. It is seen that high shear stress causes anisotropy which decreases to small values hidden in statistical noise for the lowest shear stress values. The stress-induced orientation of molecules thus cannot be a source of a significant additional error.

The final low stress calculations used systems obtained (with the exception of least elongated PEO1) by composing eight periodic copies of the small equilibrium systems. The approach to the stationary flow (monitored using the amplitude of the velocity profile) required times up to 100 ps for higher oligomers. The productive runs were 84 – 210 ps long.

It is seen that the computed viscosities are generally too low, especially for higher oligomers, even if the approximated systematic error of 10% is taken into account. This is probably caused by the united atom approximation: a real integration between hydrogens with a positive partical charge and negatively charged oxygens is not so smooth as if replaced by united $CH_2$ groups. Lower molecular dipole moments may also have some influence.

### 4.3. The *Gauche* Effect

The *gauche* effect can be studied by the probability distribution of the dihedral angle around the C—C bond. It may be interesting to compare three curves:

1. The Boltzmann probability $\exp[-E_{t\phi t}/kT]$
2. The dihedral angle distribution for one free molecule (i.e., in dilute gas phase)
3. The dihedral angle distribution in the liquid phase.

The energy $E_{t\phi t}$ is the minimized conformational energy with investigated central dihedral angle $\phi$ and with all other dihedrals in the *trans* conformation. All degrees of freedom but $\phi$ are optimized. All the distributions are normalized to give unity integral. As already mentioned, the gas results are obtained by MD with zero angular momentum. We correct this error for DME. The expected error caused by rotation for PEO6 is probably small because the molecule is large.

The results for central bond in DME and PEO6 are shown in Figures 1 and 2, respectively. In both cases the Boltzmann probability of *gauche*

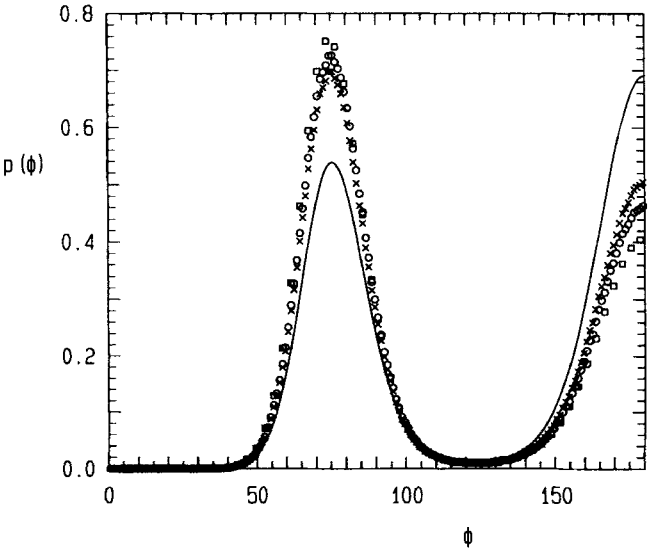


FIGURE 1 Dihedral angle distribution along the central bond C—C in dimethoxyethane at 20°C. Solid line: $\exp[-E_{t\phi t}/kT]$; crosses: MD results for one non-rotating molecule; circles: MD one-molecule results corrected for rotations; squares: liquid phase. Error bars are comparable or less than symbol sizes and are not shown.

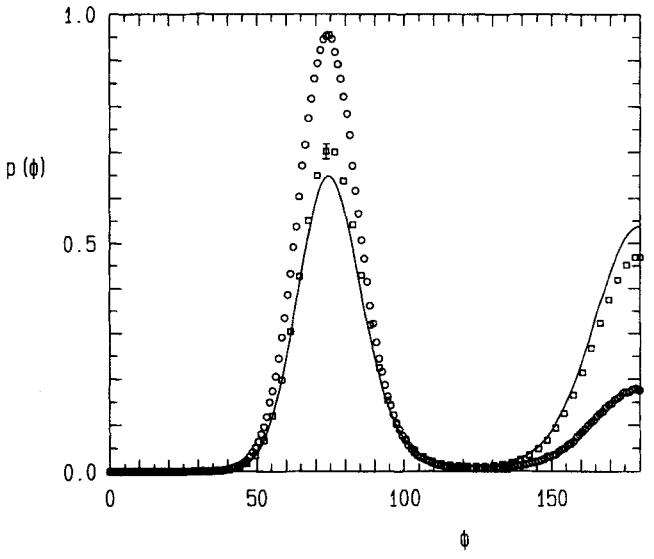


FIGURE 2 Dihedral angle distribution along the central bond C—C in PEO6 at 20°C. See Figure 1 for the explanation of the symbols. Error bars are shown for the *gauche* maxima.



conformations is lower than the gas and liquid values which is not surprising because some of the multi-*gauche* conformations have very low energy compared to *tgt*.

The influence of the liquid environment on the abundance of *gauche* conformations of the central bond $CH_2$—$CH_2$ in DME was mentioned in the Introduction. It is supported also by the present study, see Figure 1 where more *gauche* conformers in the liquid phase than in the gas phase are observed. The effect is small (less than −0.1 kcal/mol if the dihedral distributions are interpreted as Boltzmann probabilities) because of high stability of the $tg^+g^-$ conformer. Since the molecules of DME are relatively small, the steric hindrance of different parts of the molecule is low. One can then explain this *gauche* effect by the influence of positively charged $CH_2$ groups of one molecule which with higher probability lie between the oxygens of the O—C—C—O chain of another molecule, forming a pentagon.

Quantitatively the *gauche* effect is smaller (71% *gauche*) than experimentally observed [63] (83% *gauche*). It should be also noted that the rotational isomeric state analysis off NMR measurement on DME [20, 21] suggests significantly lower energies of the conformers with the central C—C bond *gauche* than are found in the *ab initio* values. If this is at least partly taken

into account and lower *gauche* energies (still within the estimated maximum error [22] of 0.2–0.3 kcal/mol) are introduced into the model, the agreement between theory and experiment improves both for DME and PEO, as discussed below.

The situation changes for higher oligomers, see Figure 2 where results for the central C—C bond of PEO6 are shown. The highest concentration of *gauche* conformers is observed for a free molecules which means that the conformers must be stabilized by intramolecular interactions (the low energy conformer $g^+g^-$ from Table IX is one of the candidates). In other words, coiled conformations are preferred. These conformations are less probable in the liquid phase (mainly for entropic reasons because the same low energy per molecule can be obtained by both coiled and uncoiled conformations) and thus the ratio of the *gauche* conformers decreases. This is further supported by the values of radius of gyration (gas 3.765(9)Å, liquid 4.82(2)Å)) and mean quadratic end-to-end distance (gas 8.58(4)Å, liquid 13.2(1) Å).

The PUFF model for free molecules of PEO oligomers predicts *gauche-trans* difference for inner C—C bonds (with all other bonds *trans*) about −0.12 kcal/mol, see Table IX. This is lower than for DME. The observed liquid dihedral angle distribution for the central bond in PEO6 corresponds to approximately −0.24 kcal/mol energy difference while the experiment-based estimate [19] is −0.4 kcal/mol.

The −0.24 kcal/mol value of the *gauche* effect is the consequence of quantum mechanical calculations of oligomer torsional energies and the adopted strategy for building the polarizable force field. We have observed how rescaling 1–5 interactions for DME led to considerable improvement of conformational equilibria and effectively corrected the lack of explicit hydrogens. One can expect that explicit hydrogens would further stabilize the pentagonal formations and improve the agreement between theory and experiment.

TABLE IX PUFF minimum energies of selected conformers of PEO6, related to the all-*trans* conformer. The conformations of C—C bonds are for clarity marked by upper case *T* and *G*

| *conformer* | $E-E_{ref}$ [*kcal/mol*] |
|---|---|
| *ttTttTttTttTtt* | 0 |
| *ttGttTttTttTtt* | −0.04 |
| *ttTttGttTttTtt* | −0.13 |
| *ttTttTttGttTtt* | −0.11 |
| *ttTttTttG*$^+$*g*$^-$*tTttTtt* | −0.36 |
| *ttTttTtgTttTtt* | 1.53 |

## 5. CONCLUSIONS

The polarizable united-atom field presented in this paper has been adjusted to *ab initio* conformational energies, experimental bulk densities, and dielectric constants. There is still a gap between molecular dipole moments and the related bulk property, i.e., the dielectric constant, but this gap is narrower than for models with pairwise additive forces.

The influence of liquid environment to the *gauche* effect is lower than predicted by most non-polarizable models [13, 35, 34] but about the same as given by the accurate *ab initio* based non-polarizable full-atom model [36]. These observations as well as the experimental findings [20, 21] support the idea that only a relatively small part of the *gauche* effect (−0.1 to −0.15 kcal/mol) is caused by the liquid environment, the rest being a quantum effect.

Molecular dynamics simulations using this PUFF (polarizable united-atom force field) quite accurately yield dielectric constants, densities, conformational populations, and shear viscosities for oligomeric ethylene oxides. Moreover, by including polarizable atoms, they provide an additional flexibility in the force field that should be important in computational study of polymer electrolyte systems, where mutual polarization of cation and Lewis base etheric oxygen is probably neccessary to describe both salt dissolution and cation diffusion.



### *Acknowledgements*

This work was supported by the LBL-DOE program on advanced batteries, the ARO, the Danish Research Councils' Decentral Parallel Computing Initiative, Odense Steel Shipyard and Novo Nordisk.

### *References*

[1] Armand, M. B., Chabagno, J. M. and Duclot, M. J. D. (1979). *Fast Ion Transport in Solids*; P. M. Vashishta, J. N. Mundy, G. K. Shenoy, Eds. (North-Holland: Amsterdam) p. 131.
[2] Gray, F. M. (1991). *Solid Polymer Electrolytes* (VCH: New York).
[3] Armand, M. B. (1986). *Ann. Revs. Mat. Sci.*, **16**, 245.
[4] Vogel, H. (1921). *Phys. Z.*, **22**, 645.
[5] Ratner, M. A. and Shriver, D. F. (1988). "Ion transport in solvent-free polymers", *Chem. Rev.*, **88**, 109.
[6] MacCallum, J. R. and Vincent, C. A. (1989). *Polymer Electrolyte Reviews 2*, (Elsevier: London).
[7] MacCallum, J. R. and Vincent, C. A. (1989). *Polymers for Electronic Applications*, J. H. Lai, Ed. (CRC: Boca Raton, Florida), p. 157.

[8] *Second International Symposium on Polymer Electrolytes*, B. Scrosati, Ed. (Elsevier) 1990.
[9] *Electrochimica Acta*, **1995**, #13/14
[10] Shriver, D. F. and Bruce, P. (1994). *Solid State Electrochemistry*, P. Bruce, Ed. (Cambridge), p. 95.
[11] Payne, V. A., Xu, J., Forsyth, M., Ratner, M. A., Shriver, D. F. and de Leeuw, S. W. (1995). "Molecular dynamics simulations of ion clustering in NaI/ether solutions. I. Effect of ion charge", *J. Chem. Phys.*, **103**, 8734; ibid p. 8746 "II. Effect of ion concentration".
[12] Olender, R. and Nitzan, A. (1994). "Lattice theory of solvation and dissociation in macromolecular fluids. II. Quasichemical approximation", *J. Chem. Phys.*, **101**, 2338.
[13] Neyertz, S., Brown, D. and Thomas, J. O. (1994). "Molecular dynamics simulation of crystalline poly (ethylene oxide)", *J. Chem. Phys.*, **101**, 10064.
[14] Müller-Plathe, F. (1994). "Permeation of polymers — A computational approach", *Acta Polym.*, **45**, 259.
[15] Lonergan, M. C., Nitzan, A., Ratner, M. A. and Shriver, D. F. (1995). "Dynamically disordered hopping, glass transition and polymer electrolytes", *J. Chem. Phys.*, **103**, 3253.
[16] Torell, L. M. and Schantz, S. (1989). *Polymer Electrolytes 2*, J. R. MacCallum and C. A. Vincent, Eds. (Elsevier: London), pp. 1–42. L. M. Torell, P. Jacobsson, G. Petersen (1993). "A Raman study of ion solvation and association in polymer electrolytes", *Polymers Adv. Tech.*, **4**, 152.
[17] Halley, J. W., unpublished.
[18] Catlow, C. R. A. and Mills, G. E. (1995). "Computer simulation of ionically conducting polymers", *Electrochimica Acta*, **40**, 2057. Mills, G. E., Catlow, C. R. A. (1994). "Ion clustering in polymer electrolytes", *J. Chem. Soc. Chem. Commun.*, **18**, 2037.
[19] Abe, A. and Mark, J. E. (1976). "Conformational energies and the random-coil dimensions and dipole moments of the polyoxides $CH_3O[(CH_2)_yO]_xCH_3$", *J. Am. Chem. Soc.*, **98**, 6468.
[20] Tasaki, K. and Abe, A. (1985). "NMR studies and conformational energy calculations of 1,2-dimethoxyethane and poly(oxyethylene)", *Polym. J.*, **17**, 641.
[21] Inomata, K. and Abe, A. (1992). "Conformation of 1,2-dimethoxyethane in the gas phase: A rotational isomeric state simulation of NMR vicinal coupling constants", *J. Phys. Chem.*, **96**, 7934.
[22] Jaffe, R. L., Smith, G. D. and Yoon, Do Y. (1993). "Conformations of 1,2-dimethoxyethane from *ab initio* electronic structure calculations", *J. Phys. Chem.*, **97**, 12745.
[23] Smith, G. D., Yoon, Do Y. and Jaffe, R. L. (1993). "A third-order rotational isomeric state model for poly (oxyethylene) based upon *ab initio* electronic structure analyses of model molecules", *Macromolecules*, **26**, 5213.
[24] Smith, G. D., Yoon, Do Y., Jaffe, R. L., Colby, R. H., Krishnamoorti, R. and Fetters, L. J. (1996). "Conformations and structues of poly (oxyethylene) melts from molecular dynamics simulations and small-angle neutron scattering experiments", *Macromolecules*, **29**, 3462.
[25] Gejji, S. P., Tegenfeld, J. and Lindgren, J. (1994). "Conformational analysis of poly(ethylene oxide) oligomers: diglyme", *Chem. Phys. Lett.*, **226**, 427.
[26] Müller-Plathe, F. and van Gunsteren, W. F. (1994). "Can simple quantum-chemical continuum models explain the gauche effect in poly (ethylene oxide)?", *Macromolecules*, **27**, 6040.
[27] Müller-Plathe, F. (1994). "How good are molecular local density methods? Case study: The quadrupole moment of benzene, geometry and electrostatics of dimethyl sulfoxide, and the conformations of dimethoxy ethane", *Braz. J. Phys.*, **24**, 965.
[28] Liu, H., Müller-Plathe, F. and van Gunsteren, W. F. (1995). "A molecular dynamics simulation study with a combined quantum mechanical and molecular mechanical potential energy function: Solvation effects on the conformational equilibrium of dimethoxyethane", *J. Chem. Phys.*, **102**, 1722.
[29] Xie, L. and Farrington, G. C. (1992). "Molecular mechanics and dynamics simulation of poly(ethylene oxide) electrolytes", *Solid State Ionics*, **53–56**, 1054.
[30] Müller-Plathe, F. and van Gunsteren, W. F. (1995). "Computer simulation of a polymer electrolyte: lithium iodide in amorphous poly (ethylene oxide)", *J. Chem. Phys.*, **103**, 4745.

[31] Müller-Plathe, F., Liu, H. and van Gunsteren, W. F. (1995). "Conceptual hierarchies in polymer electrolyte simulations– From quantum chemistry to molecular dynamics", *Comput. Polymer Sci.*, **5**, 89.
[32] Neyertz, S., Brown, D. and Thomas, J. O. (1995). "Molecular dynamics simulation of the crystalline phase of Poly (ethylene oxide) – Sodium Iodide, $PEO_3NaI$", *Electrochimica Acta*, **40**, 2063.
[33] Neyertz, S. and Brown, D. (1995). "A computer simulation study of the chain configurations in poly (ethylene oxide)-homologue melts", *J. Chem. Phys.*, **102**, 9725.
[34] Neyertz, S. and Thomas, J. O. (1995). "Molecular dynamics simulations of the amorphous polymer electrolyte $PEO_xNaI$", *Comput. Polymer Sci.*, **5**, 107.
[35] Bressanini, D., Gamba, A. and Morosi, G. (1990). "A Monte Carlo simulation of liquid 1,2-dimethoxyethane", *J. Phys. Chem.*, **94**, 4299.
[36] Smith, G. D., Jaffe, R. L. and Yoon, Do Y. (1995). "Conformations of 1,2-dimethoxyethane in the gas and liquid phases from molecules dynamics simulations", *J. Am. Chem. Soc.*, **117**, 530.
[37] Smith, G. D., Jaffe, R. L. and Yoon, Do Y. (1993). "A force field for simulations of 1,2-dimethoxyethane and poly(oxyethylene) based upon *ab initio* electronic structure calculations on model molecules", *J. Phys. Chem.*, **97**, 12752.
[38] Sprik, M. and Klein, M. L. (1988). "A polarizable model for water using distributed charge sites", *J. Chem. Phys.*, **89**, 7556.
[39] Sprik, M. (1991). "Computer simulation of the dynamics of induced polarization fluctuations in water", *J. Phys. Chem.*, **95**, 2283.
[40] Brodholdt, J., Sampoli, M. and Vallari, M. (1995). "Parameterizing a polarizable intermolecular potential for water", *Molec. Phys.*, **86**, 159.
[41] Zhu, S.-B., Yao, S., Zhu, J.-B., Singh, S. and Robinson, G. W. (1991). "A flexible/polarizable simple charge water model", *J. Phys. Chem.*, **95**, 6211.
[42] Ray, D., Feller, S., Moore, M. B., Glendenning, E. D. and Armentrout, P. B. (1996). "Cation-ether complex in the gas phase: Bound dissociation energies and equilibrium structures of $Li^+$(1,2 dimethoxyethane)$_x$, $x = 1$ and 2, and $Li^+$(12-crown-4)", *J. Phys. Chem.*, **100**, 16116.
[43] Kolafa, J. and Perram, J. W. (1992). "Cutoff errors in the Ewald summation formulae for point charge systems", *Molec. Simul.*, **9**, 351.
[44] Briggs, J. M., Matsui, T. and Jorgensen, W. L. (1990). "Monte Carlo simulations of liquid alkyl ethers with the OPLS potential functions", *J. Comput. Chem.*, **11**, 958.
[45] QUANTA *Parameter Handbook* (Polygen Corporation) (1990).
[46] Matsuura, H. and Miazawa, T. (1968). "Intrachain force field and normal vibrations of polyethylene glycol", *Bull. Chem. Soc. Japan*, **41**, 1796.
[47] Jorgensen, W. L., Madura, J. D. and Swenson, C. J. (1984). "Optimized intermolecular potential functions for liquid hydrocarbons", *J. Am. Chem. Soc.*, **106**, 6638.
[48] Brooks, B. R., Bruccoleri, R. E., Olafson, B. D., States, D. J., Swaminathan, S. and Karplus, M. (1983). "CHARMM: A program for macromolecular energy, minimization and dynamics calculations", *J. Comput. Chem.*, **4**, 187.
[49] Jorgensen, W. J. (1981). "Transferable intermolecular potential functions for water, alcohols and ethers. Application to liquid water", *J. Am. Chem. Soc.*, **103**, 335.
[50] Dunfield, L. G., Burgess, A. W. and Scheraga, H. A. (1978). "Energy parameters in polypeptides. 8. Empirical energy algorithm for the conformational analysis of large molecules", *J. Phys. Chem.*, **82**, 2609.
[51] Rappé, A. K., Casewit, C. J., Colwell, K. S., Goddard III, W. A. and Skiff, W. M. (1992). "UFF, a full periodic table force field for molecular mechanics and molecular dynamics simulations", *J. Am. Chem. Soc.*, **114**, 10024.
[52] Allen, M. P. and Tildesley, D. J. (1987). *Computer Simulations of Liquids* (Clarendon Press).
[53] Perram, J. W. and Smith, E. R. (1987). "Microscopic derivation of formulas for calculating dielectric constants by simulations", *J. Stat. Phys.*, **46**, 179.
[54] Kolafa, J. (1996). "Numerical integration of equations of motion with a self-consistent field given by an implicit equation", *Molec. Simul.*, **18**, 193.

[55] Cummings, P. T. and Evans, D. J. (1992). "Nonequlibrium molecular dynamics approaches to transport properties and non-Newtonian fluid rheology", *Ind. Eng. Chem. Res.*, **31**, 1237.
[56] Cui, S. T., Cummings, P. T. and Cochran, H. D. (1996). "Multiple step nonequilibrium molecular dynamics simulation of the rheological properties of liquid *n*-decane", *J. Chem. Phys.*, **104**, 255.
[57] Nosé, S. (1984). "A molecular dynamics method for simulations in the canonical ensemble", *Molec. Phys.*, **52**, 255; Hoover, W. G. (1985). "Canonical dynamics: equilibrium phase-space distributions", *Phys. Rev. A*, **31**, 1695.
[58] Go, N. and Scheraga, H. A. (1976). "On the use of classical statistical mechanics in the treatment of polymer chain conformation", *Macromolecules*, **9**, 535; Gunsteren, W. F. (1980). "Constrained dynamics of flexible molecules", *Mol. Phys.*, **40**, 1015.
[59] de Leeuw, S. W., Perram, J. W. and Petersen, H. G. (1990). "Hamilton's equations for constrained dynamical systems", *J. Stat. Phys.*, **61**, 1203.
[60] Vesely, F. J. (1997). "*N*-particle dynamics of polarizable Stockmayer-type molecules", *J. Comput. Phys.*, **24**, 361.
[61] Rowley, R. L. and Ely, J. F. (1992). "Note on the number dependence of nonequilibrium molecular dynamics simulation of the viscosity of structured molecules", *J. Chem. Phys.*, **96**, 4814.
[62] Chynoweth, S., Klomp, U. C. and Michopoulos, Y. (1991). "Comments on: Rheology of *n*-alkanes by nonequilibrium molecular dynamics", *J. Chem. Phys.*, **95**, 3024.
[63] Viti, V. and Zampetti, P. (1973). "Dielectric properties of 2-methoxyethanol and 1,2-dimethoxyethan. Comparison with ethylene glycol.", *Chem. Phys.*, **2**, 233.
[64] Pollock, E. L., Alder, B. J. and Patey, G. N. (1981). "Static dielectric properties of polarizable Stockmayer fluid", *Physica*, **108A**,14.
[65] Fixman, M. (1974). "Classical statistical mechanics of constraints: A theorem and application to polymers", *Proc. Nat. Acad. Sci.* USA, **71**, 3050.
[66] *CRC Handbook of Chemistry and Physics, 76th Edition* (CRC Press) (1995).
[67] Lide, D. R. (1995). *Handbook of Organic Solvents* (CRC Press).



## APPENDIX A

### Efficient Molecular Dynamics with a Self-consistent Field

Let interaction site $i$ contain a polarizable point dipole with the value of polarizability $\alpha_i$. The induced dipole $\boldsymbol{\mu}_i$ in electrostatic field $\mathbf{E}_i$ is

$$\boldsymbol{\mu}_i = \alpha_i \mathbf{E}_i \tag{12}$$

In many-particle systems the induced dipoles change the electric field so that an implicit equation

$$\mu = F(\mu) \tag{13}$$

has to be solved to obtain the self-consistent field. In (13) $\mu$ stands for all $N$ vectors $\boldsymbol{\mu}_i$, $i = 1, \ldots, N$, and any dependence of right-hand side $F$ on other degrees of freedom or time is omitted for simplicity.

Equation (13) can be solved by direct iterations [60, 64] which generally requires several evaluations of Coulomb forces in one integration step and the molecular dynamics calculations become expensive. This inefficiency can be avoided for second-order integrators (such as the popular Verlet method) provided that the values of induced dipoles are predicted using their values from previous steps [54]. In this study we use the predictor with the best energy conservation

$$\mu^p(t+h) = 2.5\mu(t) - 2\mu(t-h) + 0.5\mu(t-2h) \tag{14}$$

where $t$ denotes the time and $h$ the timestep. The corrector then must contain damping with certain mixing iteration parameter $\omega < 1$:

$$\mu(t+h) = \omega F(\mu^p(t+h)) + (1-\omega)\mu^p(t+h) \tag{15}$$

The value of $\omega = 0.6$ guarantees the stability of the predictor–corrector procedure for all physically acceptable (i.e., converging) right-hand sides $F$, through in many cases a higher value leading to lower integration errors may be used. For details of optimizing $\omega$ and other predictors we refer to the original paper [54].



## APPENDIX B

### Classical Gas-phase Calculations

Let a molecule consist of $n$ atoms. Some of the bond lengths and/or angles may be constrained; in this Appendix we assume true rigid constraints and not limits of infinitely stiff springs [58]. Instead of the usual $n$ Cartesian coordinates $\{\mathbf{r}_i\}$, $i = 1,\ldots,n$, the configuration of the molecule may be described by $m$ generalized coordinates $\mathbf{q} = \{q_A\}$, $A = 1,\ldots,m$. For example, a chain molecule with all bonds and bond angles constrained may be fully described by the three Euler angles of the first three atoms and $n-3$ torsional (dihedral) angles (and a 3D vector of the center of mass; since the integration over these three degrees of freedom is trivial, we shall omit them in the following).

The canonical expectation value of static quantity $X = X(\mathbf{q})$ is [65]:

$$\langle X \rangle = I(X)/I(1) \tag{16}$$

where

$$I(X) = \int X \exp\left[-\left(\sum_{A,B=1}^{m} p_A G_{AB} p_B + U\right)/k_B T\right] \mathbf{dpdq} \tag{17}$$

$$= \text{const} \int X \exp(-U/k_B T)(\det G)^{1/2} \mathbf{dq} \tag{18}$$

In (17), $p_A$ denotes the generalized momentum conjugate to $q_A$ and

$$G_{AB} = \sum_{i=1}^{n} m_i \frac{\partial \mathbf{r}_i}{\partial q_A} \frac{\partial \mathbf{r}_i}{\partial q_B} \tag{19}$$

is the metric tensor.

If the angular momentum is to be conserved, the integration in (17) has to be constrained to zero angular momentum **A**:

$$\mathbf{A} = \sum_{i=1}^{n} \mathbf{r}_i \times m_i \dot{\mathbf{r}}_i = \sum_{B=1}^{m} \mathbf{A}_B p_B \tag{20}$$

where

$$\mathbf{A}_B = \sum_{i=1}^{n} \mathbf{r}_i \times m_i \sum_{A=1}^{m} \frac{\partial \mathbf{r}_i}{\partial q_A} G_{AB}^{-1} \tag{21}$$

By replacing the Dirac delta function $\delta(\mathbf{A})$ (expressing the $\mathbf{A} = 0$ condition in (17)) by the limit of Gaussian function $\exp(-K|\mathbf{A}|^2)$ for $K \to \infty$, we finally get

$$I_{A=0}(X) = \text{const} \lim_{K \to \infty} \int X \exp(-U/k_B T)[\det(G^{-1} + KS)]^{-1/2} \mathrm{d}\{q\} \tag{22}$$

where

$$S_{AB} = \mathbf{A}_A \cdot \mathbf{A}_B \tag{23}$$

The integration over Euler angles in (17) and (22) may be omitted because of space isotropy. The calculations for models of diethylether and DME with bond angles constrained thus require two and three dimensional numerical integrations, respectively.

## APPENDIX C

### Fluctuation Formula for Calculating Dielectric Constant of Polarizable Systems in Periodic Boundary Conditions

The fluctuation formulas for dielectric constant can be derived by calculating the canonical ensemble averaged response caused by a small external electric field $\mathbf{e}_0$ applied to the system [53]. The only difference for the polarizable system is that the (instantaneous) response of the polarizable dipoles has to be taken into account in the total polarization. For the sake of simplicity, we assume only isotropic response; the polarizability tensor is thus diagonal and may be replaced by a scalar. Thus, the total dipole moment $\mathbf{M}_{\mathbf{e}_0}(\Omega)$ in region $\Omega$ subject to external field $\mathbf{e}_0$

$$\mathbf{M}_{\mathbf{e}_0}(\Omega) = \sum_{i\in\Omega} \mu_{\mathbf{e}_0;\, i} = \sum_{i\in\Omega} \mu_{0;\, i} + \mathbf{e}_0 \sum_{i\in\Omega} \alpha_i = \mathbf{M}_0(\Omega) + \mathbf{e}_0 A(\Omega) \tag{24}$$

where

$$A(\Omega) = \sum_{i\in\Omega} \alpha_i \tag{25}$$

is the total polarizability of region $\Omega$, has to replace formula (7) of Ref. [53]. By following the derivation and by using the same assumption we get the generalization of Eq. (11) of Ref. [53] for the mean polarization $\mathbf{p}$ in region $\Omega$:

$$V(\Omega)\langle 4\pi \mathbf{p}(\Omega)\rangle_{\mathbf{e}_0} = 4\pi\left(A + \frac{\langle \mathbf{M}_0(\Omega)\cdot \mathbf{M}_0\rangle_0}{3k_BT}\right)\mathbf{e}_0 + \mathrm{O}(\mathbf{e}_0^2) \tag{26}$$

By identifying region $\Omega$ with the simulation box and by and using Eqs. (26)–(28) of Ref. [53], we obtain the final formula for the dielectric constant (relative to vacuum)

$$\frac{(\varepsilon_r - 1)(1 + 2\varepsilon')}{\varepsilon_r + 2\varepsilon'} = \xi \quad \text{or} \quad \varepsilon_r = \frac{1 + 2\varepsilon'(1 + \xi)}{1 + 2\varepsilon' - \xi} \tag{27}$$

where

$$\xi = \frac{4\pi}{V}\frac{\langle \mathbf{M}^2\rangle_0}{3k_BT} + A \tag{28}$$

The dielectric constant $\varepsilon'$ of the surrounding continuum is a free parameter (remember that it appears in the expression for the electrostatic potential, see (23) of Ref. [53]) and the measured dielectric constant $\varepsilon_r$ should not (in the thermodynamic limit) depend on it. This is actually a very strong test for the correctness of the calculations, especially if $\varepsilon_r$ is high and small $\varepsilon'$ is used, because the denominator in (27) is then a difference of big numbers.